Terahertz Dynamics of a Topologically Protected State: Quantum Hall Effect Plateaus near the Cyclotron Resonance of a Two-Dimensional Electron Gas

A. V. Stier,[1] C. T. Ellis,[1] J. Kwon,[1] H. Xing,[1] H. Zhang,[1] D. Eason,[1] G. Strasser,[1] T. Morimoto,[2] H. Aoki,[2] H. Zeng,[1] B. D. McCombe,[1] and J. Cerne[1]

[1]*Department of Physics, University at Buffalo, The State University of New York, Buffalo, New York 14260, USA*

[2]*Department of Physics, University of Tokyo, Hongo, Tokyo 113-0033, Japan*

(Received 1 May 2015; published 8 December 2015)

We measure the Hall conductivity of a two-dimensional electron gas formed at a GaAs/AlGaAs heterojunction in the terahertz regime close to the cyclotron resonance frequency using highly sensitive Faraday rotation measurements. The sample is electrically gated, allowing the electron density to be changed continuously by more than a factor of 3. We observe clear plateaulike and steplike features in the Faraday rotation angle vs electron density and magnetic field (Landau-level filling factor) even at fields or frequencies very close to cyclotron resonance absorption. These features are the high frequency manifestation of quantum Hall plateaus—a signature of topologically protected edge states. We observe both odd and even filling factor plateaus and explore the temperature dependence of these plateaus. Although dynamical scaling theory begins to break down in the frequency region of our measurements, we find good agreement with theory.

DOI: 10.1103/PhysRevLett.115.247401 PACS numbers: 78.20.Ls, 71.10.Ca, 73.43.Lp, 76.40.+b

The dc quantum Hall effect (QHE) [1] has critically shaped our understanding of the physics of two-dimensional systems. This remarkable effect is the first example of a topologically protected state [2,3]; the transverse Hall conductivity σ_{xy} is quantized by the suppression of backscattering in the quantum Hall edge channels. In spite of great progress in understanding the physics of the QHE, one particularly important question remains unanswered: How does the static Hall conductivity evolve into the dynamical (optical) Hall conductivity $\sigma_{xy}(\omega)$? This has been partially addressed by experimental [4–11] and theoretical [12,13] investigations. According to the localization picture, the QHE emerges from the coexistence of localized and delocalized states in disorder-broadened Landau levels (LL) [14]. The QHE plateau-to-plateau transition takes place over an energy interval W each time the Fermi energy passes from one localized region of the density of states of a particular LL to another via delocalized states near the peak in the density of states [14]. When a critical energy E_c, which is located at the center of each disorder-broadened LL is approached, the localization length ξ diverges as a power law $\xi(E) \sim |E - E_c|^{-\gamma}$. At zero frequency [2], the distinction between localized and delocalized states is clear; other than the topologically protected edge states, only states with localization length ξ larger than the sample size L can carry a dc current. For high frequency driving electric fields, the distinction is less clear, as both localized and delocalized states can contribute to the conductivity, with the localized states oscillating about their localization centers. When the amplitude of the oscillations of delocalized states becomes smaller than the dc ξ, localized and delocalized states become indistinguishable, and the signature of the QHE, the plateaus, disappears. Finite frequency ω and temperature T effectively shrink L and modify the plateau-to-plateau transition width W (see Supplemental Material [15]). In this case, W is given by $W \sim T^{\kappa}$ and $W \sim \omega^{\kappa}$, where $\kappa = 1/z\gamma$ and therefore the components of the conductivity tensor exhibit a scaling behavior. Noninteracting electron systems [13,16,17] as well as systems with short range interactions [18] are governed by a dynamical exponent $z = 2$; long-range interactions change the exponent to $z = 1$ [19]. Studies of the GHz longitudinal conductivity $\sigma_{xx}(\omega)$ reveal a scaling behavior with a critical exponent of $\kappa = 0.5 \pm 0.1$, yielding a dynamical exponent of $z = 0.9 \pm 0.1$ [4,6]. This scaling picture is only valid in the low frequency region ($\omega \ll \omega_c$), and thus does not necessarily address the situation of the dynamical response close to cyclotron resonance (CR). Morimoto *et al.* have provided theoretical evidence that the steplike structure of the static Hall conductivity should survive even in the THz regime (1 THz $= 10^{12}$ Hz, 4.22 meV, 33 cm^{-1}), despite the dynamical response being dominated by strong absorptive optical transitions between adjacent LLs [long orange arrow in Fig. 1(a)] rather than weak intra-LL transitions [short blue arrow in Fig. 1(a)] [12]. Experimental work to test these predictions has been limited. Microwave measurements at magnetic fields where the radiation frequency (ω) is far below the cyclotron resonance frequency (ω_c), $(\omega/\omega_c) \ll 1$, have shown plateaus in $\sigma_{xy}(\omega)$ up to 33 GHz [4,20], and a universal scaling in $\sigma_{xx}(\omega)$ up to 55 GHz [5,6]. More recently, time domain THz spectroscopy was used [7] to measure $\sigma_{xy}(\omega)$ on an ungated GaAs/AlGaAs heterojunction, focusing on the region $\omega \approx 0.2$–$0.8\omega_c$,

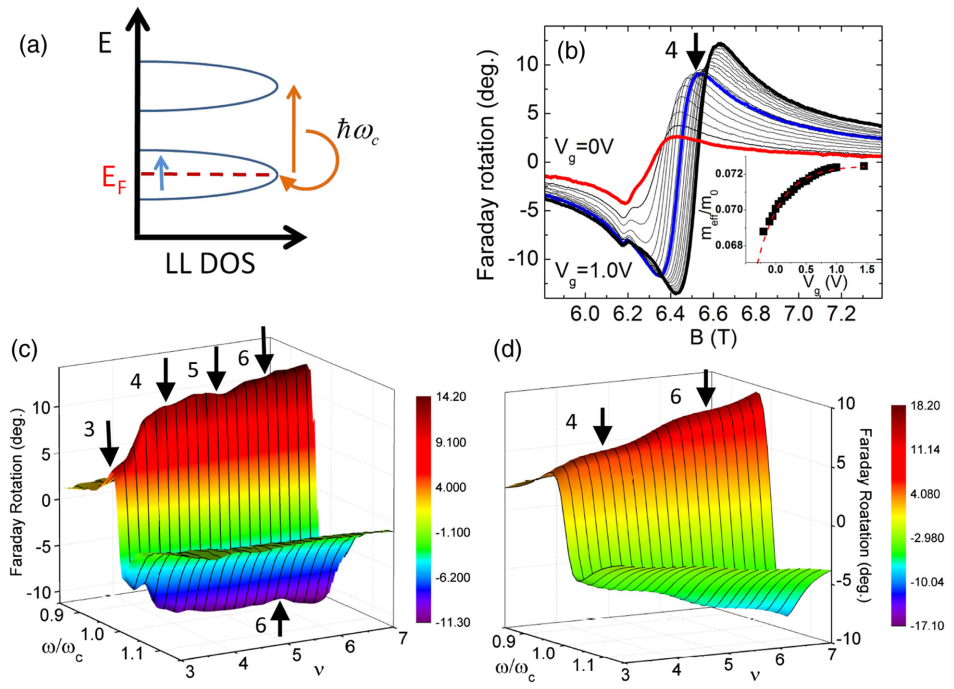

FIG. 1 (color online). (a) Diagram of Drude-like intraband transitions (blue arrow) and circularly active CR interband transitions (orange arrow) between adjacent LL. (b) Faraday rotation for $\omega_{\mathrm{THz}} = 2.52$ THz vs magnetic field B at various, fixed gate voltages V_g. The large background is due to CR. The inset shows the shift of effective electron mass as a function of V_g. (c) The measured Faraday rotation for $\omega_{\mathrm{THz}} = 3.14$ THz vs B at various fixed V_g translated into the parameter space $[(\omega/\omega_c), \nu]$. Integer filling factor positions are labeled with black arrows. (d) Theoretical predictions of $\theta_F[(\omega/\omega_c), \nu]$ showing the plateau structure at similar filling factors. The calculation neglects spin splitting (which we show occurs for our system) and therefore only shows spin-degenerate plateaus at even Landau level filling factors.

which corresponds to a probe frequency that is more than 7 linewidths away from CR, and shows an inflection point in $\sigma_{xy}(\omega)$ near filling factor 2. This inflection point was interpreted as a QHE plateau. Clear plateaulike behavior associated with the QHE nearer CR has yet to be observed and explored in spite of literally hundreds of publications on CR in GaAs two-dimensional electron gases (2DEGs) since 1985 [21]. Recent results on the THz QHE [9] and infrared magnetopolarimetry at CR [9,22,23] in graphene further motivate our work.

We use a highly sensitive polarization-modulation technique to measure the Faraday angle of a 2DEG at the interface of a GaAs/AlGaAs heterostructure in the THz regime close to CR $[(\omega/\omega_c) \cong 1]$ [24]. In the thin-film limit, the Faraday angle θ_F (the rotation of the plane of polarization of the electric field of the transmitted light) is directly proportional to the optical Hall conductivity through $\theta_F(\omega) + i\eta(\omega) \simeq [1/(1+n_s)c\epsilon_0]\sigma_{xy}(\omega)$ [7,25,26]. The line shape of the optical Hall conductivity around CR is given by the Drude expression, $\sigma_{xy}(\omega) = (ne^2/m_{\mathrm{eff}})[\omega_c/(i\omega + i/\tau)^2 - \omega_c^2]$. In this region of strong CR absorption and dispersion we observe multiple clear and robust plateaulike and steplike features in the Faraday rotation angle vs electron density and B. These features appear near the expected regions of density and B that correspond to QHE plateaus at integer filling factors.

The system studied is a 2DEG formed at the interface of a GaAs/AlGaAs heterojunction $[n_{2\mathrm{D}}(V_g = 0) = 5.7 \times 10^{11}\ \mathrm{cm}^{-2}$, $\mu = 1.7 \times 10^5\ \mathrm{cm}^2/\mathrm{Vs}$ at $T = 77$ K]. For these parameters, there is small density (~3%) of electrons in the first excited subband even at $V_g = 0$. At higher positive V_g, both subbands need to be taken into account (see Sec. II of the Supplemental Material [15]). We use monochromatic emission lines from an optically pumped molecular gas laser and a polarization-modulation technique [24,25] (see Sec. IV of the Supplemental Material [15]) to probe the Faraday angle, at two frequencies 2.52 and 3.14 THz, with a sensitivity better than 0.1°. The high signal-to-noise ratio of these measurements allows us to investigate the scaling of the σ_{xy} plateaus with both frequency and temperature, and to compare it with theory [6,12,13].

Figure 1 summarizes our key results. The Faraday angle θ_F measured at 2.52 THz and $T = 1.6$ K is shown in Fig. 1(b) as a function of B for a series of constant gate voltages (V_g). Two resonances are observed: a strong resonance feature that is consistent with predictions from the Drude model for CR in a 2DEG and a smaller feature near 6.2 T, which we associate with residual bulk carriers in the sample substrate. The inflection point of the large dispersive resonance feature marks the position of CR. The shift in position of the resonance feature to higher B as V_g

and carrier density increase is consistent with an increase in the effective mass due to band nonparabolicity [27] [see the inset of Fig. 1(b)]. We determine the 2D electron density n_{2D} as a function of V_g using dc Hall measurements on samples in the van der Pauw geometry. The measured n_{2D} agrees well with a simple capacitor model using the measured sample parameters. This allows us to translate our data into the parameter space $[(\omega/\omega_c), \nu]$, where the cyclotron frequency $\omega_c = (eB/m_{\text{eff}})$ and filling factor $\nu = (n_{2D}h/eB)$. Figure 1(c) shows θ_F measured at a higher THz frequency, $\omega_{\text{THz}} = 3.14$ THz, plotted vs ω/ω_c and ν. The black arrows in Figs. 1(b)–1(d) mark the positions of integer filling factors. The $\nu = 4$ feature is very clear in Fig. 1(b), where the positive peak height of several Faraday CR curves remains constant over a significant range of V_g. Note the plateaulike features at $\nu = 3$ and 4 as well as a clear step at $\nu = 3.5$ on the top ridgeline, and $\nu = 6$ on the bottom (minimum) ridgeline in the data in Fig. 1(c). Note that the features on the ridgelines are well within the CR linewidth and that the $\nu = 6$ feature on the bottom ridgeline corresponds to a probing radiation energy that is higher than the CR energy. We attribute these features to QHE plateaus that we observe in the THz Faraday rotation, which are described in greater detail in Figs. 2–3 and the Supplemental Material [15]. Note that both even and odd filling factor features are observed in the Faraday measurements. To compare our measured results with numerical calculations, we adopt the equation of motion (EOM) method [28], where optical conductivities are described through EOM of the current density and disorder effects are treated as a phenomenological broadening for LLs. Theoretical calculations for a LL broadening $(\Gamma/\hbar\omega_c) = 0.03$ are shown in Fig. 1(d) and are in reasonable qualitative and quantitative agreement with the measurements. Specifically, simulation and experiment agree in the magnitude of θ_F and reproduce well the filling factor dependence at a particular ω/ω_c [see Fig. 2(a)] for even filling factors. The calculations assume that the Zeeman splitting is negligible and therefore each LL is spin degenerate, containing both spin-up and spin-down electrons [29].

We have further investigated θ_F as a function of V_g at a series of constant B above CR $(\omega_c > \omega)$, which corresponds to changing ν at constant B. Before we discuss the results in detail, we compare the THz data with dc measurements [see Fig. 2(a)]. Similar to results from [6], we find that THz and dc results generally track each other [the curves are offset in Fig. 2(a) for clarity]. The dc data in Fig. 2(a) are taken at a slightly higher temperature of 1.9 K and involve sweeping B at constant V_g. As a result, the higher ν plateaus in the dc data are taken at smaller B (resulting in smaller LL and spin splittings) so the spin-split plateaus are weakened compared to the 1.6 K measurements that sweep V_g at a higher B. Although the $\nu = 3$

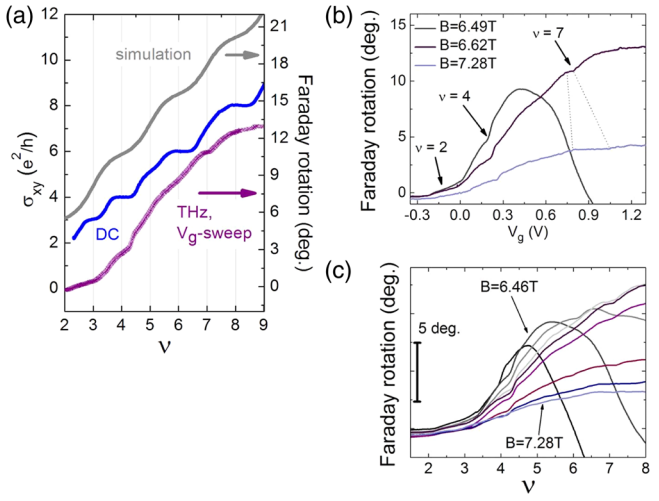

FIG. 2 (color online). (a) THz Faraday measurements (purple symbols) at 2.52 THz and 6.62 T, dc Hall conductance measurements (blue line), and a numerical THz Faraday simulation plotted as functions of the filling factor ν. Weak $\nu = 3$, 5, 6, and 8 as well as strong $\nu = 4$ and $\nu = 7$ plateau features are seen. Curves are offset for clarity. Numerical simulation for $(\Gamma/\hbar\omega_c) = 0.03$ is shown by the gray solid line. Note that the numerical simulations explicitly assume spin degenerate Landaus levels, and hence only show even filling factor plateaus. (b) and (c) Faraday rotation vs V_g and filling factor ν for various fixed magnetic fields, increasing in increments of ~0.1 T from 6.46 to 7.28 T.

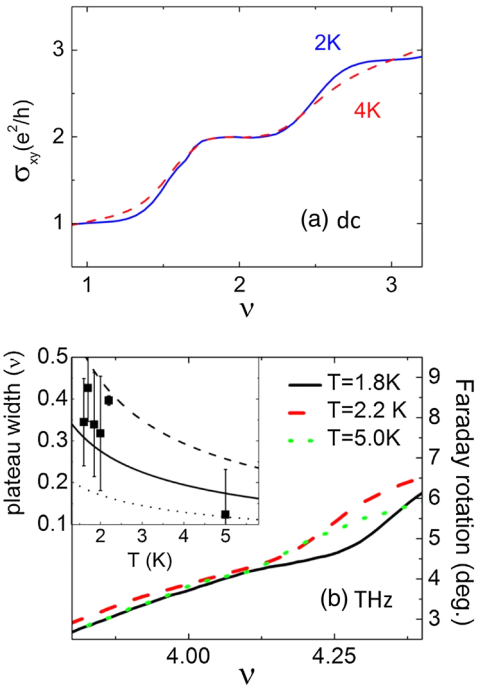

FIG. 3 (color online). (a) Measured dc Hall conductance vs filling factor for $T = 2$ K (blue solid) and $T = 4$ K (red dashed) at a density of $n_{2D} = 5.5 \times 10^{11}$ cm^{-2}. (b) THz Faraday rotation as a function of filling factor at $(\omega/\omega_c) = 0.97$ and at $T = 1.8$ K (black solid line), $T = 2.2$ K (red dashed line), and $T = 5.0$ K (green dotted line). The inset shows the plateau width as a function of temperature. Lines are calculated after [6] with exponent $\kappa = 0.5$ (solid), $\kappa = 0.6$ (dashed), and $\kappa = 0.4$ (dotted).

plateau is very clear in the dc data, higher odd filling factor plateaus at $\nu = 5$ and to a much lesser extent at $\nu = 7$ are still visible. One would not expect to see odd filling factor plateaus in bulk GaAs at the T and B used in our measurements due to the small bulk g factor. However, in a GaAs/AlGaAs 2DEG the g factor is significantly enhanced due to the many-body exchange interaction [30,31]. We estimate the enhanced g factor to range between 6.6–5.9 from the lowest $(5 \times 10^{11}\ \mathrm{cm}^2)$ to the highest carrier densities $(\sim 10^{12}\ \mathrm{cm}^2)$, respectively. This results in a spin gap of approximately 2.5 meV (30 K) at 7 T. At 1.6 K and 7 T, the spin splitting and the LL splitting of 11 meV (130 K) will both produce well-resolved plateaus, and we expect to see clearly spin-split LLs and thus plateaus at both even and odd filling factors. This is seen in the THz θ_F data in Fig. 2(a), especially for data that are recorded far away from CR. In THz θ_F data we see clear plateaus at $\nu = 4$ and 7, as well as weaker features at $\nu = 3$, 5, 6, and 8. Figure 2(b) shows the THz θ_F vs V_g at several fixed B. The QHE plateaus ride on the overall broad cyclotron resonance dispersion feature. Most notable is the evolution of the $\nu = 7$ plateau, which is washed out close to CR (6.49 T) and evolves into a distinct and broad plateau for increasing B above CR. Very close to CR at 6.46 T, electron heating through the strong resonant absorption of THz radiation is likely responsible for the disappearance of the plateaus. Note also how the V_g positions for the $\nu = 4$ and 7 plateaus shift with B. This is expected since the carrier density at which these plateaus occur grows with increasing B. Figure 2(c) shows the THz θ_F as a function of ν at various fixed B. We observe a pronounced plateau-step feature for $\nu = 4$ for all B fields. Note that in this case, the position of the $\nu = 4$ plateau does not shift horizontally as B increases. The overall magnitude of this feature diminishes for decreasing ω/ω_c, because the Drude background upon which it rides decreases. The Faraday signal is larger close to CR, which improves the signal-to-noise ratio and therefore our ability to detect THz QHE plateaus. The plateau for $\nu = 5$ is barely visible as a slight inflection in the $\theta_F(\omega)$ vs ν data. In contrast the next higher filling factor plateau $\nu = 6$ is discernible very close to CR, but it then smears out and becomes comparable to the $\nu = 5$ plateau at higher B. Note that the vertical spacing between plateaus (or where the Faraday data cross integer filling factor values) is not uniform. Since the Hall conductance is proportional to the Faraday angle, nonuniform spacing in θ_F implies that the THz Hall conductance is not quantized, which is one of the main predictions by Ref. [12]. Although B and ω are fixed during the V_g sweeps, ω_c decreases slightly with increasing V_g due to the increase in effective mass with carrier density. As a result, ω/ω_c approaches unity despite B and ω being constant, and CR absorption becomes stronger as V_g and ν increase. This is most clearly seen in the V_g scans at lower B in Fig. 2(c), where the θ_F background drops at higher ν, following the classical Faraday rotation dispersive line shape at CR.

Several plateaus are weak or missing under certain conditions. We attribute some of this behavior to the overlap of LLs in the first excited subband with LLs in the ground subband. A qualitative explanation of this effect is provided in Sec. 2 of the Supplemental Material [15].

The observed THz plateau structures are sensitive to temperature as depicted in Fig. 3. The temperature dependence of the odd filling factor plateaus $\nu = 1$ and 3 for dc magnetotransport is consistent with the temperature dependence of the exchange enhanced g factor. As shown in Fig. 3(a), the odd plateaus quickly smear out as temperature increases from 2 to 4 K, while the even plateau at $\nu = 2$ remains nearly unchanged. We also clearly see even filling factor plateaus in dc measurements at 9 K. On the other hand, Fig. 3(b) shows that the THz $\nu = 4$ plateau at $(\omega/\omega_c) = 0.97$ strongly depends on temperature, disappearing by 5 K. The plateau width is plotted in the inset. We can describe the decrease of the plateau width using a power law with an exponent of $\kappa = 0.5 \pm 0.1$, which is consistent with temperature scaling behavior in the GHz regime [6] and points towards an electron-electron interaction mechanism for the temperature dependence of even plateaus in the THz regime. Note that the washing out of the THz plateau cannot be solely attributed to thermal effects since the energy splitting responsible for the plateau is approximately 11 meV (130 K), which is significantly larger than $k_B T$ at 5 K.

In conclusion, we have observed clear steplike and plateaulike features close to even and odd integer filling factors in the THz $\sigma_{xy}(\omega)$. Results are analyzed with and compared to recent calculations. Unlike previous GHz and THz studies of $\sigma_{xy}(\omega)$, where the probing radiation was more than 7 resonance linewidths below the cyclotron resonance, it is remarkable that in our measurements where the photons are less 0.5 linewidths away from resonance and strong optical absorption occurs, the dc QHE effect is found to persist. In fact, the $\nu = 6$ feature on the bottom ridgeline in Fig. 1(c) suggests that QHE plateaus may even be observed for $\omega > \omega_c$. It is interesting to observe that the polarization of THz photons close to inter-Landau level (cyclotron) absorption is sensitive to whether the Fermi energy lies in localized or delocalized levels, producing QHE plateaus. The temperature scaling of the THz plateau widths is consistent with electron-electron interaction processes.

This work was supported by NSF-DMR1006078 (C. T. E. and J. C.), NSF-MWN1008138 (A. V. S. and B. D. M.), NSF DMR1104994 (H. X. and H. Zeng), NSF CBET-1510121 (H. X. and H. Zeng); H. A. has been supported in part by a Grant-in-Aid for Scientific Research No. 23340112 from MEXT and T. M. by JSPS. We gratefully acknowledge M. Pakmehr and

A. Mukherjee for preliminary dc magnetotransport measurements. We thank M. Grayson for critical advice on processing gates for the samples used in the final dc magnetotransport measurements. We also thank S. Ganapathy for helpful discussions on the QHE.

[1] K. v. Klitzing, G. Dorda, and M. Pepper, Phys. Rev. Lett. **45**, 494 (1980).
[2] J. E. Avron, D. Osadchy, and R. Seiler, Phys. Today **56**, 38 (2003).
[3] D. J. Thouless, M. Kohmoto, M. P. Nightingale, and M. den Nijs, Phys. Rev. Lett. **49**, 405 (1982).
[4] F. Kuchar, R. Meisels, G. Weimann, and W. Schlapp, Phys. Rev. B **33**, 2965 (1986).
[5] L. W. Engel, D. Shahar, Ç. Kurdak, and D. C. Tsui, Phys. Rev. Lett. **71**, 2638 (1993).
[6] F. Hohls, U. Zeitler, R. J. Haug, R. Meisels, K. Dybko, and F. Kuchar, Phys. Rev. Lett. **89**, 276801 (2002).
[7] Y. Ikebe, T. Morimoto, R. Masutomi, T. Okamoto, H. Aoki, and R. Shimano, Phys. Rev. Lett. **104**, 256802 (2010).
[8] A. V. Stier *et al.*, *AIP Conf. Proc.* 1399, 627 (2011).
[9] R. Shimano, G. Yumoto, J. Y. Yoo, R. Matsunaga, S. Tanabe, H. Hibino, T. Morimoto, and H. Aoki, Nat. Commun. **4**, 1841 (2013).
[10] R. Shimano, Y. Ikebe, K. S. Takahashi, M. Kawasaki, N. Nagaosa, and Y. Tokura, Europhys. Lett. **95**, 17002 (2011).
[11] G. S. Jenkins, D. C. Schmadel, and H. D. Drew, Rev. Sci. Instrum. **81**, 083903 (2010).
[12] T. Morimoto, Y. Hatsugai, and H. Aoki, Phys. Rev. Lett. **103**, 116803 (2009).
[13] T. Morimoto, Y. Avishai, and H. Aoki, Phys. Rev. B **82**, 081404 (2010).
[14] H. Aoki and T. Ando, Solid State Commun. **38**, 1079 (1981).
[15] See Supplemental Material at http://link.aps.org/supplemental/10.1103/PhysRevLett.115.247401 for detailed description on how the QHE plateaus are determined, the occupation of the second subband effects some QHE plateaus, experimental details, scattering mechanisms and a detailed discussion on frequency and temperature scaling in the quantum Hall regime.
[16] B. M. Gammel and W. Brenig, Phys. Rev. B **53**, R13279 (1996).
[17] J. T. Chalker, J. Phys. C **21**, L119 (1988).
[18] D.-H. Lee and Z. Wang, Phys. Rev. Lett. **76**, 4014 (1996).
[19] D. G. Polyakov and B. I. Shklovskii, Phys. Rev. B **48**, 11167 (1993).
[20] V. A. Volkov *et al.*, Pis'ma Zh. Eksp. Teor. Fiz. **43**, 255 (1986) [JETP Lett. **43**, 326 (1986)].
[21] Based on a Web of Science topic search using "GaAs cyclotron resonance" which returned 1211 papers (30 December 2011).
[22] C. T. Ellis *et al.*, in *Proceedings of the37th International Conference on Infrared, Millimeter, and Terahertz Waves (IRMMW-THz), 2012*, p. 1.
[23] C. T. Ellis *et al.*, Sci. Rep. 3 (2013).
[24] D. K. George, A. V. Stier, C. T. Ellis, B. D. McCombe, J. Černe, and A. G. Markelz, J. Opt. Soc. Am. B **29**, 1406 (2012).
[25] M. Grayson, L. B. Rigal, D. C. Schmadel, H. D. Drew, and P.-J. Kung, Phys. Rev. Lett. **89**, 037003 (2002).
[26] Interestingly, Drude calculations show that at lower carrier densities such as in our GaAs/AlGaAs 2DEG, $\theta_F \propto \sigma_{xy}$, while in higher density metallic systems $\theta_F \approx \theta_H$ in the THz range, where $\theta_H = \sigma_{xy}/\sigma_{xx}$ is the Hall angle.
[27] T. Ando, J. Phys. Soc. Jpn. **51**, 3893 (1982).
[28] A. Ferreira, J. Viana-Gomes, Yu. V. Bludov, V. Pereira, N. M. R. Peres, and A. H. Castro Neto, Phys. Rev. B **84**, 235410 (2011).
[29] Note that in Figs. 1(c) and 1(d), θ_F decreases as ω/ω_c approaches zero. By converting our dc σ_{xx} and σ_{xy} measurements into a dc (frequency approaching zero) θ_F we can compare the dc and THz values of θ_F. Our measured dc θ_F is about 0.1°, which is more than 2 orders of magnitude smaller than the THz θ_F that we measure near the cyclotron frequency. This is consistent with a simple Drude model.
[30] D. R. Leadley, R. J. Nicholas, J. J. Harris, and C. T. Foxon, Phys. Rev. B **58**, 13036 (1998).
[31] I. L. Aleiner and L. I. Glazman, Phys. Rev. B **52**, 11296 (1995).